Energy materials

Effect of annealing temperature on microstructure and thermoelectric transport properties of Cu$_{2.1}$Zn$_{0.9}$SnSe$_4$ alloys

Fahad Mehmood[1], Hongchao Wang[1,*] , Wenbin Su[1], Mahwish Khan[1], Taichang Huo[1], and Chunlei Wang[1,*]

[1] School of Physics, State Key Laboratory of Crystal Materials, Shandong University, Jinan, China

ABSTRACT

Cu-based quaternary chalcogenide compounds have been thermoelectric topic of interest among researchers, especially in recent years, due to their intrinsically low thermal conductivity. Recently plenty of work is done on thermoelectric properties of Cu$_2$ZnSnSe$_4$-based alloys emphasizing on importance of Cu$_2$ZnSnSe$_4$-based alloys in thermoelectric power generation. In this study, we report the effect of annealing temperature on microstructure and thermoelectric properties of Cu$_{2.1}$Zn$_{0.9}$SnSe$_4$ alloys. Cu$_{2.1}$Zn$_{0.9}$SnSe$_4$ compounds were synthesized by high-temperature melting followed by annealing at four different temperatures (600 °C, 650 °C, 700 °C and 725 °C). X-ray diffraction combined with Raman spectroscopy confirmed the presence of Cu$_2$ZnSnSe$_4$ phase along with ZnSe and CuSe secondary phases. The increased annealing temperature critically affected the microstructure of Cu$_{2.1}$Zn$_{0.9}$SnSe4 alloys. Successive increase in annealing temperature subsequently increases the average grain size from 7.3 for 600 sample to 12.1 μm for 725 °C sample by shifting grain size distribution toward higher range. Increased grain size results in reduced carrier scattering and decreases the electrical resistivity eventually improving power factor and maximum power factor of about 400 μWk^{-2} m^{-1} is obtained for 725 °C sample. Besides, the increased annealing temperature resulted in increased thermal conductivity attributing increased grain size resulting in low phonon scattering. 725 °C sample shows highest power factor and moderate thermal conductivity among all the samples which resulted in highest value of figure of merit for 725 °C sample of about 0.1 at 673 K.

Ⓐ Springer

GRAPHICAL ABSTRACT
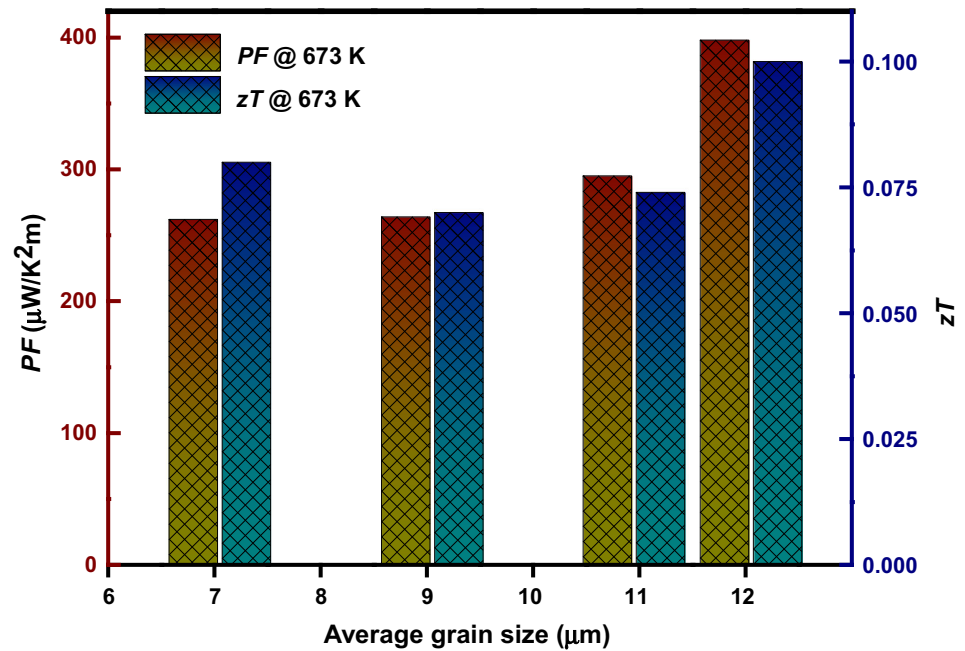
Introduction

$Cu_2ZnSnSe_4$(CZTSe) compounds have been exclusively known for their wide applications in thin-film solar cells with certified solar conversion efficiencies around 12% due to their electronic structure and optical response [1]. Recently $Cu_2ZnSnSe_4$-based quaternary chalcogenide compounds have drawn significant interest as potential candidate for thermoelectric materials due to its intrinsically low thermal conductivity which is featured by its complex crystal structure [2–5]. In last decade, thermoelectric properties of CZTSe compounds have been extensively explored and various strategies have been employed to enhance the thermoelectric performance of CZTSe compounds, e.g. introduction of extra charge carriers through p-type doping, band gap engineering, grain boundary engineering and introduction of structural distortions are to name the few [2, 4, 6, 7].

Previous reports have successfully demonstrated drastic enhancement in thermoelectric properties of CZTSe compounds by converting insulating $ZnSe_4$ paths to conducting path ways through Cu-rich composition. The replacement of Zn by Cu element tremendously increased the electrical conductivity for $Cu_{2.1}Zn_{0.9}SnSe_4$ alloys. This significant increase in electrical conductivity resulted in dramatic enhancement in power factor and dimensionless figure of merit [3, 6]. In another similar work, Dong et al. have measured the thermoelectric properties of $Cu_2ZnSnSe_4$ compounds with 15% and 20% Cu doping at Zn site. They achieved improved power factor and reduced thermal conductivity simultaneously attributing enhanced electrical conductivity and increased phonon scattering [8]. Besides Cu doping, another strategy to enhance the power factor is the replacement of Se with heavier element 'Te'. Te alloying enhanced the power factor and reduced the thermal conductivity simultaneously which resulted in improved figure of merit of 0.56 at 700 K [9]. Furthermore, thermoelectric properties of CZTSe compounds synthesised by different techniques have been explored in literature, e.g. solid state reaction, hot-injection synthesis, hydrothermal synthesis, solid state reaction accompanied with ball milling,

colloidal synthesis, combustion synthesis [3, 10–13]. Solid-state synthesis method for preparation of CZTSe bulk samples has been reported for different annealing times and temperatures, e.g. annealing at 773 K for 48 h, 773 K for 172 h, 873 K for one week, 973 K for 96 h, 973 K for one week and 1073 K for 96 h [9, 10, 14–16]. Difference in synthesis conditions such as reaction temperature, reaction holding time, annealing temperature and annealing time could lead to different microstructure, hence affecting thermoelectric properties. In addition it is well known that microstructure can significantly affect the electrical and thermal transport properties. Thus, it is important to study the effect of annealing temperature on microstructure and thermoelectric properties to optimize the synthesis conditions.

In this work, we have studied the effect of annealing temperature on thermoelectric transport properties of $Cu_{2.1}Zn_{0.9}SnSe_4$ alloys. Different annealing temperatures resulted in different microstructures, as the annealing temperature increased smaller grains merged into each other and the average grain size increased which reduced the charge carrier scattering subsequently reducing the values of electrical resistivity with the rising annealing temperature. The reduced electrical resistivity and moderate Seebeck coefficient resulted in maximum power factor of 400 $\mu WK^{-2}\ m^{-1}$ for 725 °C sample at 673 K which is about 1.5 times the value of power factor for 600 °C sample. Moreover, pores and bumps were observed on the surface of 725 °C sample which shift thermal conductivity of 725 °C sample to the lower values. Eventually, a maximum figure of merit of about 0.1 has been obtained for 725 °C sample at 673 K.

Materials and methods

$Cu_{2.1}Zn_{0.9}SnSe_4$ bulk samples were obtained through melting and annealing process of high purity elements Cu (shots, 99.5%), Zn (cylinders, 99.99%), Sn (shots, 99.9999%) and Se (shots, 99.99%). All the elements were loaded in the carbon coated quartz tube and heated to 1170 K for 6 h under vacuum. The samples were then annealed at four different temperatures 600 °C, 650 °C, 700 °C and 725 °C for 96 h by dropping the temperature to the desired value within 24 h. The obtained ingots were then hand milled into powder and loaded into 12.7 mm

graphite mold for densification at 873 K for 1 h under 70 Mpa uniaxial pressure.

Powder X-ray diffraction patterns were collected using Rigaku Smartlab 3KW X-ray diffractometer to examine the phase purity of the samples. Raman Spectra were recorded at room temperature using Confocal Raman Spectrometer (LabRAM-HR800) equipped with 633 nm laser. Scanning electron microscopy was performed on the fractured surfaces of the bulk samples to analyze the microstructure using SEM, JSM-6701F. LINSEIS (LSR-3) instrument was used to measure electrical resistivity and Seebeck coefficient of rectangular shaped samples in helium atmosphere with experimental uncertainties of ± 3% and ± 4% for electrical resistivity and Seebeck coefficient, respectively [17]. Densities of the samples were determined through Archimedes method. Thermal diffusivity coefficient and heat capacity were measured through laser flash technique by DLF-1200, TA instrument. The dimensionless figure of merit (zT) was calculated by using above-mentioned parameters. The experimental uncertainties for thermal diffusivity, heat capacity and density were ± 3%, ± 5% and ± 1%, respectively [17].

Results and discussion

Figure 1a shows the powder X-ray diffraction patterns of all the samples which shows kesterite phase $Cu_2ZnSnSe_4$ compound along with CuSe as minor secondary phase at 30.5° and 31.1° shown in Fig. 1b. Since XRD alone cannot clearly distinguish between CZTSe phase and some other chalcogenide phases ($ZnSe$, Cu_2Se, Cu_2SnSe_4) due to the overlapping of their main phase peaks [18] and the presence of secondary phases can significantly affect the electrical and thermal transport properties so in order to confirm the phase purity Raman spectroscopy was performed on 725 °C sample. The Lorentz fit of Raman spectroscopy, shown in Fig. 2, depicts the major peak located at 181 cm^{-1} which is allocated to CZTSe main phase [4, 19] and ZnSe secondary phase peaks located at 205 cm^{-1} at 252 cm^{-1} [20]. Furthermore, the presence of CuSe secondary phase present in XRD results is not detected in Raman Spectra, as a strong peak located at around 262 cm^{-1} associated with CuSe is not present in our Raman spectra [21–23], which may be due to the low concentration of CuSe phase. Hence, the combined analysis of X-ray

Figure 1 **a** XRD patterns of $Cu_{2.1}Zn_{0.9}SnSe_4$ sample with different annealing temperature and **b** enlarged XRD patterns of $Cu_{2.1}Zn_{0.9}SnSe_4$ samples with different annealing temperature.
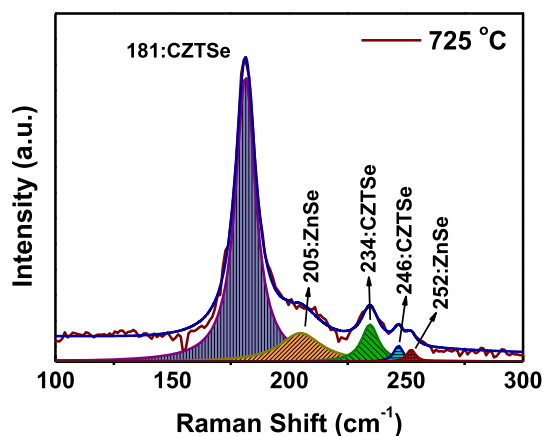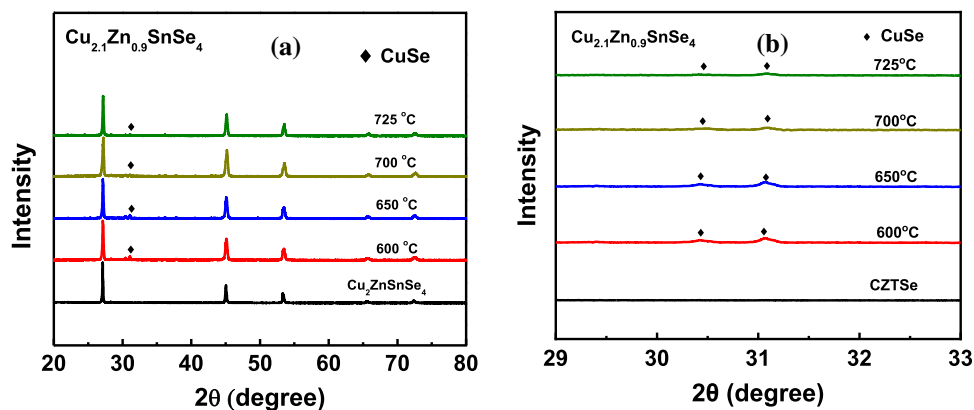
Figure 2 Raman spectra of $Cu_{2.1}Zn_{0.9}SnSe_4$ bulk sample annealed at 725 °C.

Table 1 The lattice parameters and density parameters of the $Cu_{2.1}Zn_{0.9}SnSe_4$ samples with different annealing temperature

sample	600 °C	650 °C	700 °C	725 °C
a/b (Å)	5.692	5.693	5.695	5.690
c (Å)	11.336	11.335	11.334	11.338
ρ_E (g/cm^3)	5.659	5.584	5.642	5.618
ρ_T (g/cm^3)	5.670	5.670	5.670	5.670
ρ_R (%)	99	98	99	99

diffraction and Raman spectra confirms that the samples have CZTSe main phase and ZnSe as major and CuSe as minor secondary phases. The lattice parameters 'a' and 'c' of all the specimens are shown in Table 1. The values of lattice parameters are well consisted with the reported values and remain almost unchanged for all the specimens [24].

SEM images of fractured surfaces and grain size distribution histograms of 600 °C, 650 °C, 700 °C and 725 °C samples are shown in Fig. 3 SEM image of 600 °C sample shows highly compact microstructure with comparatively higher frequency of smaller grains (3 and 5 μm) having an average grain size of ~ 7.3 μm. As the annealing temperature gradually increases to 650 °C, 700 °C and 725 °C, the smaller grains fuse into each other to form bigger grains with rising frequency of bigger grains and the average grain size gradually increases to ~ 9.3 μm, ~ 11.4 μm and ~ 12.1 μm, respectively. It depicts that higher annealing temperature enhances the grain growth and smaller grains tend to fuse into each other at higher temperature to form dense microstructure. Furthermore, SEM image of 725 °C sample shows few bumps and pores on grains surfaces, as depicted in Fig. 3e, which could possibly be created due to the Se evaporation attributing high-temperature annealing. Furthermore, Fig. 4 shows the EDS image of hot-pressed 725 °C sample which depicts non-uniform elemental distribution. Some areas show Zn-enrichment; meanwhile Cu and Sn deficiencies can also be observed. Furthermore, all elements are uniformly distributed on the remaining areas. Since Zn-rich area only contains Zn and Se elements, as depicted by EDS image, so the non-homogeneity can be attributed to the presence of ZnSe secondary phase. Hence highly dense and compact heterogeneous samples with relative densities greater than 98% are obtained as shown in Table 1.

Temperature dependence of ρ values for all the samples is shown in Fig. 5a. The electrical resistivity of 600 °C sample exhibits semi-metallic behavior in the first half and metallic behavior in the second half as the values of electrical resistivity decrease with increasing temperature up to 473 K and then increase sharply with the rising temperature which probably
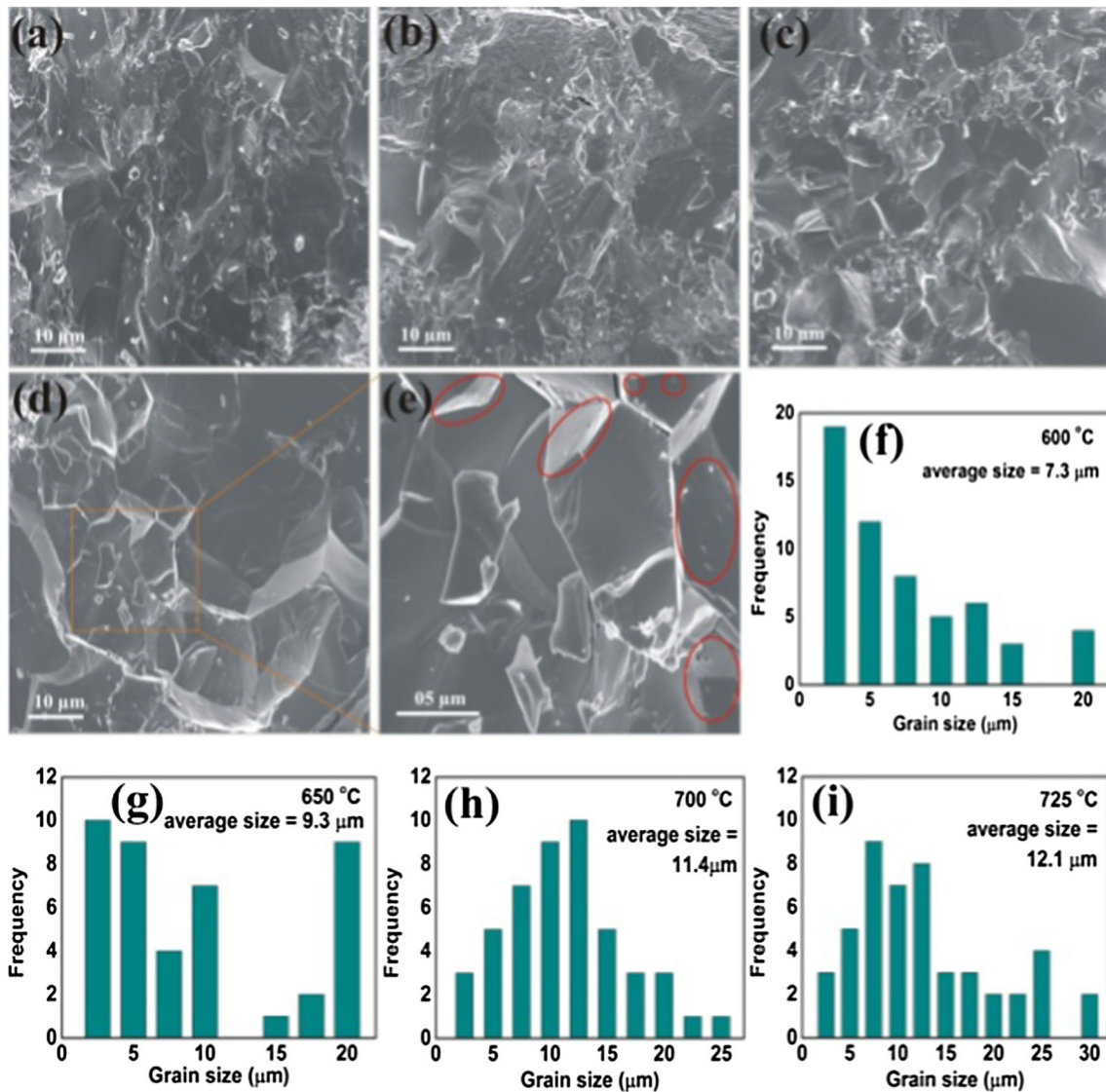
Figure 3 SEM images of fractures for $Cu_{2.1}Zn_{0.9}SnSe_4$ samples with different annealing temperature **a** 600 °C, **b** 650 °C, **c** 700 °C, **d** 725 °C, **e** enlarged image of 725 °C sample and grain size distribution of **f** 600 °C, **g** 650 °C, **h** 700 °C and **i** 725 °C samples.

be resulted from ionized impurity scattering; meanwhile the values of electrical resistivity of other samples show slight increase with the increasing temperature exhibiting degenerate semiconducting behavior [25]. Temperature dependence of electrical resistivity of 600 °C sample is different from other samples but is consistent with previous reports [8, 9, 19]. Furthermore, the electrical resistivity of the samples decreases with the increasing annealing temperature. The decrease in electrical resistivity with increased annealing temperature can be attributed to increased carrier mobility, since the higher annealing temperature tends to enhance the grain growth, as depicted by SEM images, resulting in

lesser grain boundaries to scatter charge carrier which leads to lower electrical resistivity. 725 °C sample exhibits the lowest value of electrical resistivity for the entire measured temperature range among all the samples with maximum resistivity value of about 2 mΩcm at 673 K which is about 2.2 times lower than the value of 600 °C sample (4.46 mΩcm). The values of electrical resistivity of the samples in this study are higher (especially for the samples with low annealing temperatures) as compared to the reported values for $Cu_{2.1}Zn_{0.9}SnSe_4$ sample [3] which is due to the presence of ZnSe secondary phase. Since ZnSe has significantly higher electrical resistivity (4.16–30.1 Ωcm at 300 K) as

Figure 4 SEM and EDS elemental mapping images of the polished surfaces of the $Cu_{2.1}Zn_{0.9}SnSe_4$ samples with 725 °C annealing.
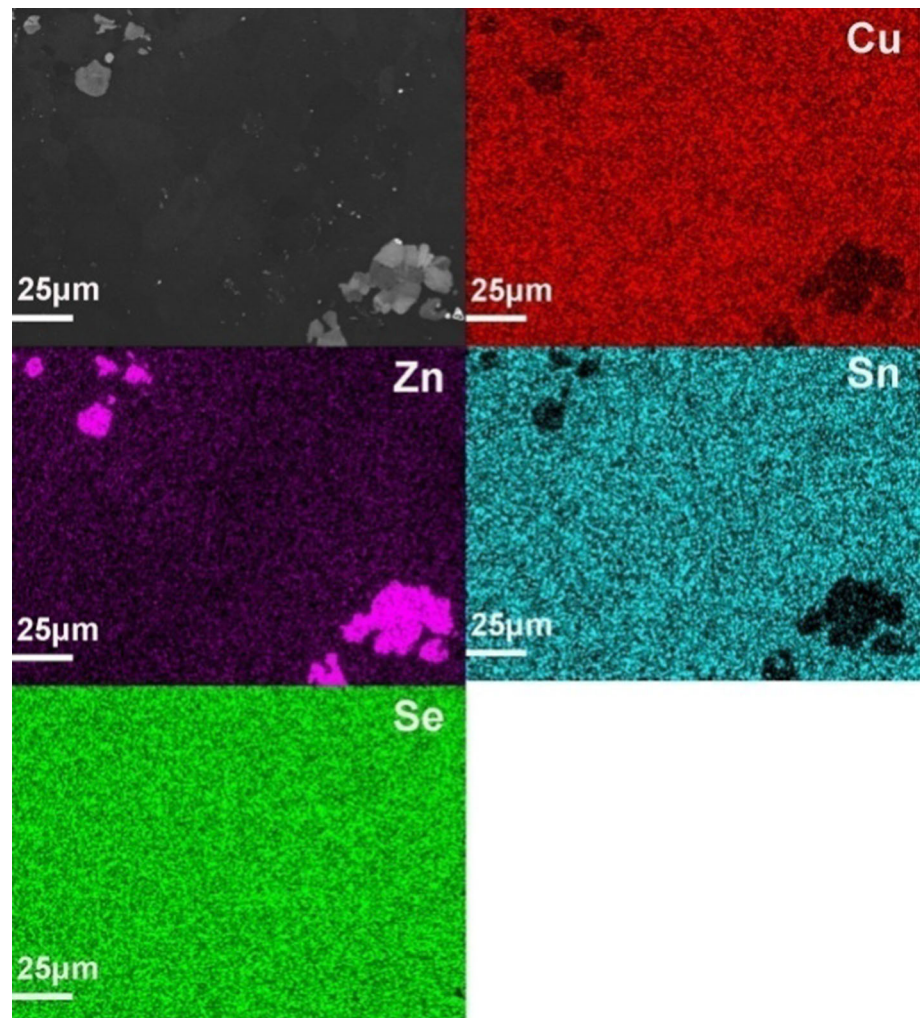

compared to CZTSe [26], so its presence increases the electrical resistivity values of the samples.

The values of Seebeck coefficient of all the samples are positive and increase almost linearly with the rising temperature as shown in Fig. 5b. The increasing annealing temperature decrease Seebeck coefficient values; meanwhile, when the annealing temperature raised to 725 °C, the value of Seebeck coefficient increased again to the value closer to 650 °C sample. Since both electrical resistivity and Seebeck coefficient contribute to the power factor, hence the increasing trend of Seebeck coefficient and little increase in electrical resistivity with increasing temperature result in increased power factor values with the rising measuring temperature for entire measured temperature range as shown in Fig. 5c. Furthermore, the increasing annealing temperature, until 650 °C, does not make significant contribution to the power factor and 600 °C and 650 °C samples

show almost similar values of power factor. This is due to the fact that while electrical resistivity decreases with increasing annealing temperature, Seebeck coefficient also decreases and the same magnitude change in both factors compensates each other resulting in no appreciable improvement in power factor of 600 °C and 650 °C samples. Meanwhile 700 °C sample shows little improvement in the power factor at 673 K. Furthermore, lowest electrical resistivity and moderate Seebeck coefficient of 725 °C sample among all the samples significantly enhance the power factor. The maximum value of power factor of about 400 $\mu WK^{-2}\,m^{-1}$ at 673 K is obtained which is 1.5 times higher than the value of 600 °C sample. Figure 5d depicts the power factor values at 673 K as a function of average grain size for all the samples. It is clearly shown that as the average grain size increases from 7.3 to 9.3 µm, the power factor does not show any change; meanwhile increase in

Figure 5 Temperature dependence of **a** electrical resistivities, **b** Seebeck coefficients, **c** power factors for $Cu_{2.1}Zn_{0.9}SnSe_4$ samples with different annealing temperature and **d** relation between average grain size and *PF* value at 673 K **e** estimated charge carrier concentrations and mobility of CZTSe alloys.
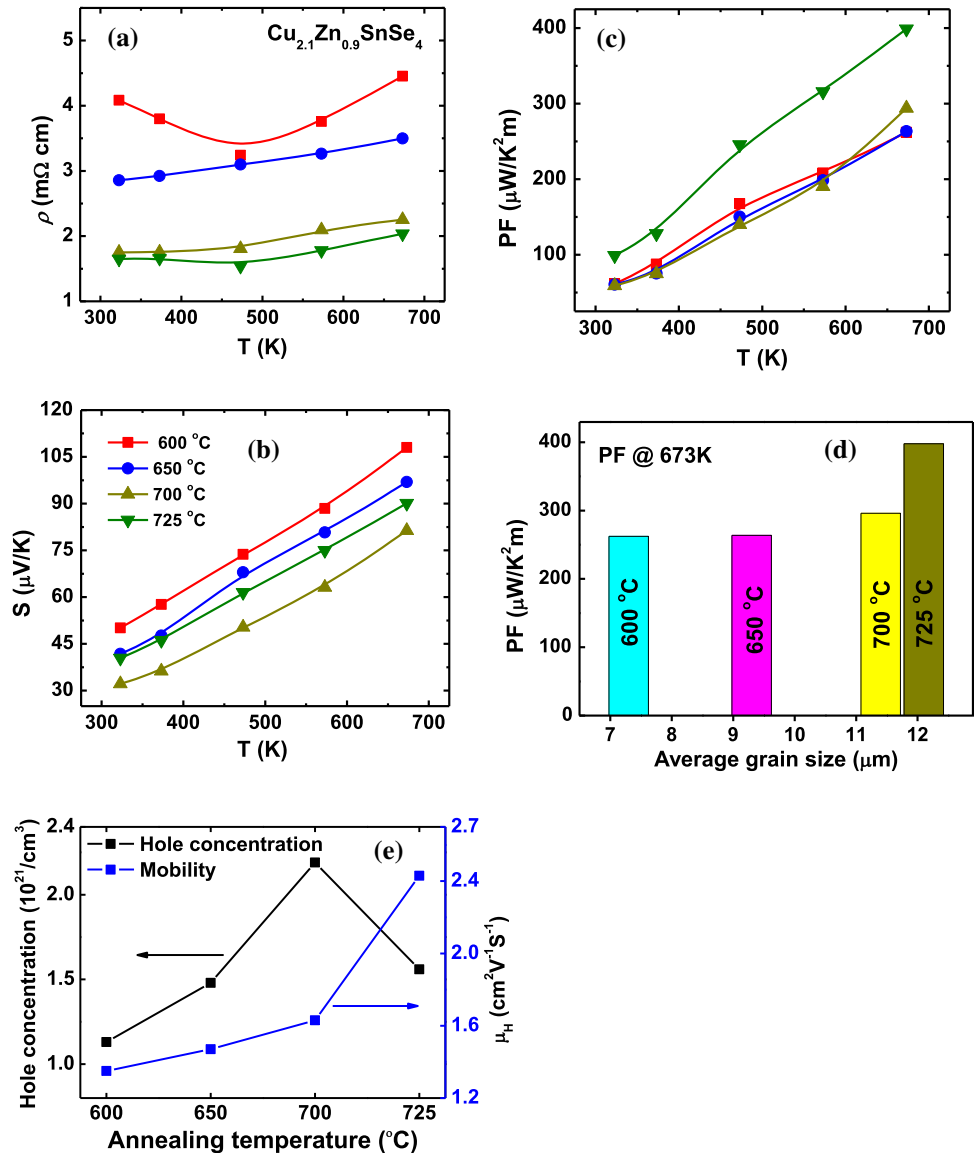
grain size to 11.4 μm exhibits a little rise in power factor value. Furthermore, with the increase in grain size to 12.1 μm, the power factor value shows a significant increase to a value of around 400 μWK^{-2}-m^{-1} attributing lowest value of electrical resistivity and moderate Seebeck coefficient.

The charge carrier density is significantly important to clearly understand the effect of annealing temperature of electrical properties. However, despite our several attempts, we couldn't get measured values of charge charier concentration for CZTSe alloys by our home made and commercial Hall measurement equipment due to the large contact resistance and inhomogeneous distributions of

samples. So, a rough estimation of charge carrier density has been obtained from Mott's formula:

$$S_d(T > \theta_D) = (\pi k_B)^2 2m^* T / e\hbar^2 (3n\pi^2)^{2/3}$$

where $m^* = 0.82m_e$ is carrier mass for $Cu_{2.1}Zn_{0.9}SnSe_4$ calculated from reported n and S values of Ref [6], e is carrier charge, k_B is Boltzmann constant, $\hbar$ is Planck's constant, T is temperature, and n is the charge carrier density [27]. The estimated Hall mobility was calculated using $\mu_H = 1/ne\rho$ and the estimated charge carrier density and Hall mobility at room temperature is shown in Fig. 5e. The hole concentration increases with the rise in annealing temperature until 700 °C and reaches its maximum value of $2.2 \times 10^{21} \ cm^{-3}$, but as the annealing temperature

raised further to 725 °C, it shows a little drops to 1.5×10^{21} cm^{-3}. In addition, it can be clearly seen that mobility value increases from 1.3 to 2.43 cm^{2}V^{-1} s^{-1} with the rise in annealing temperature from 600 to 725 °C which is in accordance with the fact that electrical resistivity decreases with the rising annealing temperature.

Total thermal conductivity of all the samples, which is depicted in Fig. 6a, decreases rapidly with the increasing temperature attributing predominant phonon scattering. Besides, the increased annealing temperature has adverse effect on thermal conductivity of the samples and the thermal conductivity increases with the rising annealing temperature attributing increase in lattice and carrier thermal conductivity with rising annealing temperature. In addition 725 °C sample exhibits thermal conductivity values similar to 650 °C sample at low temperatures and similar to 700 °C sample at high temperatures attributing lower lattice thermal conductivity of 725 °C as compared to 650 °C and 700 °C samples. The carrier thermal conductivity is estimated by using Wiedemann–Franz law $\kappa_c = LT/\rho$ where L is Lorenz constant calculated by $L = 1.5 + \exp(-|S|/116)$ [28] and ρ is electrical resistivity and lattice thermal conductivity of all the samples is estimated

by subtracting carrier thermal conductivity from total thermal conductivity. Lattice thermal conductivity of all the samples, depicted in Fig. 6b, decreases rapidly with the rising temperature which is attributed to predominant phonon scattering at high temperatures. Furthermore, the lattice thermal conductivity of the samples increases with the increasing annealing temperature which can be ascribed to increased average grain size at higher annealing temperatures, as depicted by SEM images, since increased grain size provides less grain boundary area to scatter phonon hence increasing lattice thermal conductivity. In addition, lattice thermal conductivity of 725 °C sample is lower than 650 °C and 700 °C samples, which is attributed to the presence of bumps and pores on the grain surfaces which can effectively scatter the phonons resulting in reduced lattice thermal conductivity of 725 °C sample. The relationship between average grain size and lattice thermal conductivity values at 673 K is shown in Fig. 6d. As the grain size increases from 9.3 to 11.4 μm, the lattice thermal conductivity values increase attributing reduced phonon scattering due to lesser grain boundaries. In addition, as the average grain size increases to 12.1 μm, the lattice thermal conductivity exhibits slight decrease

Figure 6 Temperature dependence of **a** the total thermal conductivities, **b** the lattice thermal conductivities and **c** carrier thermal conductivities for Cu$_{2.1}$Zn$_{0.9}$SnSe$_4$ samples with different annealing temperature and **d** lattice thermal conductivity as a function of average grain size.
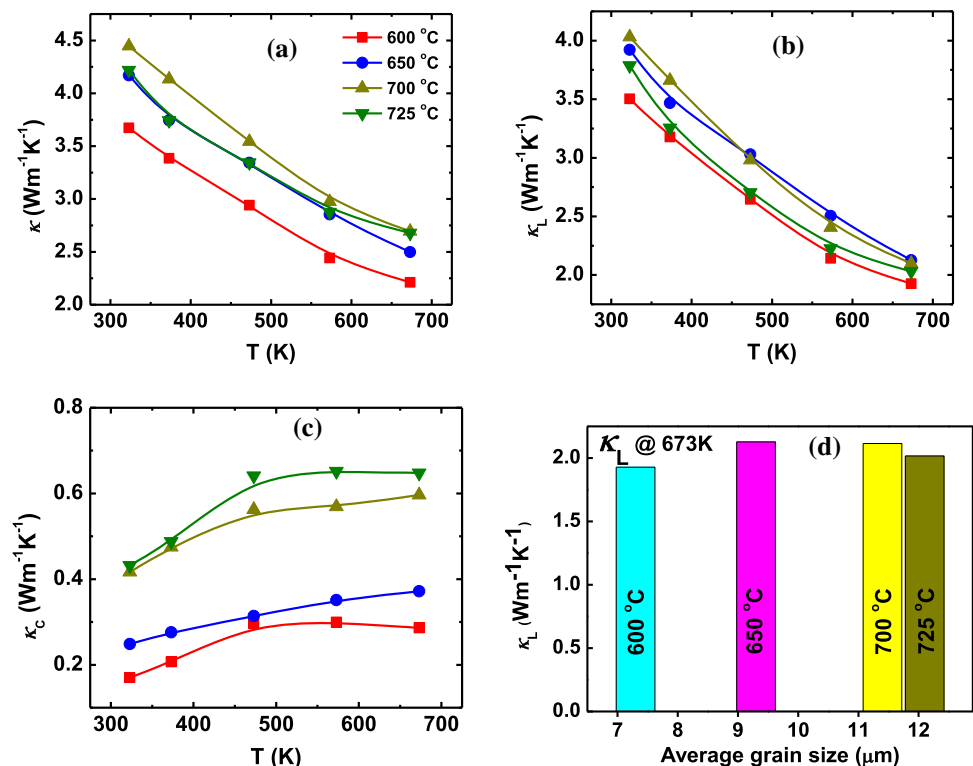
attributing pours and bumps on grains surfaces which are clearly depicted in Fig. 3e.

The temperature-dependant carrier thermal conductivity, which is electronic counter part of lattice thermal conductivity, is shown in Fig. 6c in the temperature range of 300–700 K. Carrier thermal conductivity of all the samples increases with the rising temperature for the entire temperature range. Furthermore, the contribution of carrier thermal conductivity significantly increases with the increasing annealing temperature which is obvious since higher annealing temperature reduces electrical resistivity values resulting in significantly higher contribution to the carrier thermal conductivity. Since both carrier and lattice thermal conductivities increase as the annealing temperature increases from 600 to 700 °C resulting in increased total thermal conductivity. In addition, 725 °C sample has lattice thermal conductivity lower than 650 °C and 700 °C sample and carrier thermal conductivity not too higher than 700 °C sample which leads to total thermal conductivity of 725 °C sample similar to 650 °C at lower temperatures and similar to 700 °C at highest temperatures. Furthermore, the values of total thermal conductivity in this study are higher as compared to the reported values for $Cu_{2.1}Zn_{0.9}SnSe_4$ composites [3] which is attributed to the presence of ZnSe secondary phase. Thermal conductivity of ZnSe ($19\ Wm^{-1}\ K^{-1}$) is significantly higher as compared to CZTSe compound so the presence of ZnSe secondary phase may lead to significant increase in thermal conductivity of the compound [29].

The thermoelectric figure of merit of all the samples is shown in Fig. 7a. The values of dimensionless figure of merit of all the samples increase nonlinearly with the rising temperature for the whole temperature range. The increase in annealing temperature up to 700 °C results in decreased figure of merit due to

similar power factors and enhanced thermal conductivity with rising annealing temperature, besides a further rise in the annealing temperature to 725 °C enhance the figure of merit. Since 725 °C sample has highest power factor and moderate thermal conductivity among all the samples which enhance the figure of merit and maximum value of zT of 0.1 is achieved for 725 °C sample at 673 K. In addition, dimensionless figure of merit as a function of average grain size is shown in Fig. 7b. It can be clearly seen that as the grain size increases up to 11.4 μm, the figure of merit decreases due to enhanced thermal conductivity and similar power factor; meanwhile as the average grain size increases to 12.1 μm, the figure of merit significantly increases attributing comparatively higher power factor and intermediate thermal conductivity. Comparing with reported results of $Cu_{2.1}Zn_{0.9}SnSe_4$ alloy, it is easy to find that our figure of merit is lower than reported values. The figure of merit, zT = 0.45, is reached for $Cu_{2.1}Zn_{0.9}SnSe_4$ with purity phase at 700 K [6]. It is observed that when the secondary phases like $Cu_{1.05}Zn_{0.95}$, ZnSe and so on are included, the figure of merit is down in $Cu_{2.1}Zn_{0.9}SnSe_4$ composition [30]. In our work, the secondary phases of ZnSe, CuSe are found in sample as above description, and the synthesis conditions are also different with reported work; these factors affect the electrical and thermal transports and then lead to lower figure merit. So desired purity phase and optimized synthesized conditions will be focused. Based on above results, our study provides a good insight on annealing temperature effect on microstructure and thermoelectric transport properties of CZTSe alloys. Further work could be done on effect of annealing duration on CZTSe alloys thermoelectric performance.

Figure 7 Figure of merit, zT **a** as a function of temperature for $Cu_{2.1}Zn_{0.9}SnSe_4$ samples with different annealing temperature and **b** as a function of average grain size.
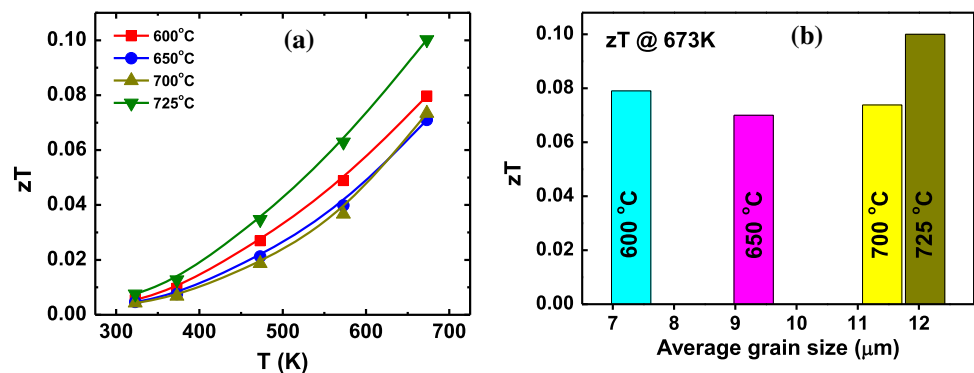
Conclusion

In this work, we have investigated the effect of annealing temperature on microstructure and thermoelectric transport properties of $Cu_{2.1}Zn_{0.9}SnSe_4$ alloys. We find out that with increasing annealing temperature small grains fuse into each other to form bigger grains and grain size distribution shifts toward higher values with higher frequency of bigger grains. The average grain size was increased from 7.3 to 12.1 μm by increasing annealing temperature from 600 to 725 °C resulting in enhanced electrical and thermal conductivity attributing reduced carrier and phonon scattering. Furthermore, the increased annealing temperature from 600 to 700 °C reduced the figure of merit due to similar power factor but enhanced the thermal conductivity. In addition when the annealing temperature was raised to 725 °C, the microstructure shows some bumps and pores on grains surface which increased phonon scattering hence reduced the thermal conductivity. Furthermore, we have observed that with increasing average grain size, power factor value increases attributing low charge scattering. Dimensionless figure of merit observed a little decrease with increasing grain size from 7.3 to 11.4 μm and then showed significant increase with further rise in grain size to 12.1 μm. Eventually highest zT value of 0.1 was obtained for 725 °C sample at 673 K attributing highest power factor and moderate thermal conductivity among all the samples.

Declarations

Conflict of interests   There are no conflict to declare.

References

[1] Lee YS, Gershon T, Gunawan O, Todorov TK, Gokmen T, Virgus Y, Guha S (2015) $Cu_2ZnSnSe_4$ Thin-film solar cells by thermal co-evaporation with 11.6% efficiency and improved minority carrier diffusion Length. Adv Energy Mater 5:1401372

[2] Li Z, Zhang W, Gu B, Zhao C, Ye B, Xiao C, Xie Y (2021) Vacancy cluster-induced local disordered structure for the enhancement of thermoelectric property in $Cu_2ZnSnSe_4$. J Mater Chem A 9:1006–1013

[3] Chen D, Zhao Y, Chen Y, Wang B, Wang Y, Zhou J, Liang Z (2015) Hot-injection synthesis of Cu-Doped Cu2ZnSnSe4 nanocrystals to reach thermoelectric zT of 0.70 at 450 °C. ACS Appl Mater Interfaces 7:24403–24408

[4] Zheng X, Liu Y, Du Y, Sun Y, Li J, Zhang R, Li Q, Chen P, Zhao G, Fang Y, Dai N (2018) P-type quaternary chalcogenides of $Cu_2ZnSn(S, Se)_4$ nanocrystals: large-scale synthesis, bandgap engineering and their thermoelectric performances. J Alloy Compd 738:484–490

[5] Huo T, Mehmood F, Wang H, Su W, Wang X, Chen T, Zhang K, Feng J, Wang C (2020) Thermoelectric properties of low Te concentration-doped $Cu_2ZnSnSe_4$-based quaternary alloys. Phys Status Solidi (A) 217:2000198

[6] Liu M-L, Huang F-Q, Chen L-D, Chen I-W (2009) A wide-band-gap p-type thermoelectric material based on quaternary chalcogenides of Cu2ZnSnQ4 (Q=S, Se). Appl Phys Lett 94:202103

[7] Zhu Y, Liu Y, Tan X, Ren G, Yu M, Hu T, Marcelli A, Xu W (2018) Enhanced thermoelectric performance through grain boundary engineering in quaternary chalcogenide $Cu_2ZnSnSe_4$. AIP Adv 8:045218

[8] Dong Y, Wang H, Nolas GS (2014) Synthesis and thermoelectric properties of Cu excess $Cu_2ZnSnSe_4$. Phys Status Solidi (RRL) Rapid Res Lett 8: 61–64

[9] Dong Y, Eckert B, Wang H, Zeng X, Tritt TM, Nolas GS (2015) Synthesis, crystal structure, and transport properties of $Cu_{2.2}Zn_{0.8}SnSe_{4-x}Te_x$ (0.1 ≤ x ≤ 0.4). Dalton Trans 44:9014–9019

[10] Shi XY, Huang FQ, Liu ML, Chen LD (2009) Thermoelectric properties of tetrahedrally bonded wide-gap stannite compounds $Cu_2ZnSn_{1-x}In_xSe_4$. Appl Phys Lett 94:122103

[11] Raju C, Falmbigl M, Rogl P, Yan X, Bauer E, Horky J, Zehetbauer M, Mallik RC (2013) Thermoelectric properties of chalcogenide based $Cu_{2+x}ZnSn_{1-x}Se_4$. AIP Adv 3:032106

[12] Fan F-J, Wang Y-X, Liu X-J, Wu L, Yu S-H (2012) Large-Scale colloidal synthesis of non-stoichiometric $cu_2znsnse_4$ nanocrystals for thermoelectric applications. Adv Mater 24:6158–6163

[13] Liu G, Li J, Chen K, Li Y, Zhou M, Han Y, Li L (2016) Direct fabrication of highly-dense $Cu_2ZnSnSe_4$ bulk materials by combustion synthesis for enhanced thermoelectric properties. Mater Des 93:238–246

[14] Zhu Y, Liu Y, Ren G, Tan X, Yu M, Lin Y-H, Nan C-W, Marcelli A, Hu T, Xu W (2018) Lattice dynamics and thermal conductivity in $Cu_2Zn_{1-x}Co_xSnSe_4$. Inorg Chem 57:6051–6056

[15] Wei K, Beauchemin L, Wang H, Porter WD, Martin J, Nolas GS (2015) Enhanced thermoelectric properties of $Cu_2ZnSnSe_4$ with Ga-doping. J Alloy Compd 650:844–847

[16] Dong Y, Wang H, Nolas GS (2013) Synthesis, crystal structure, and high temperature transport properties of p-type $Cu_2Zn_{1-x}Fe_xSnSe_4$. Inorg Chem 52:14364–14367

[17] Wei T-R, Guan M, Yu J, Zhu T, Chen L, Shi X (2018) How to measure thermoelectric properties reliably. Joule 2:2183–2188

[18] Shavel A, Arbiol J, Cabot A (2010) Synthesis of quaternary Chalcogenide nanocrystals: stannite $Cu_2Zn_xSn_ySe_{1+x+2y}$. J Am Chem Soc 132:4514–4515

[19] Mehmood F, Wang H, Su W, Khan M, Huo T, Chen T, Chebanova G, Romanenko A, Wang C (2021) Enhanced power factor and figure of merit of $Cu_2ZnSnSe_4$-based thermoelectric composites by Ag alloying. Inorg Chem 60:3452–3459

[20] Salomé PMP, Fernandes PA, da Cunha AF (2009) Morphological and structural characterization of $Cu_2ZnSnSe_4$ thin films grown by selenization of elemental precursor layers. Thin Solid Films 517:2531–2534

[21] Juškėnas R, Niaura G, Mockus Z, Kanapeckaitė S, Giraitis R, Kondrotas R, Naujokaitis A, Stalnionis G, Pakštas V, Karpavičienė V (2016) XRD studies of an electrochemically co-deposited Cu–Zn–Sn precursor and formation of a $Cu_2ZnSnSe_4$ absorber for thin-film solar cells. J Alloy Compd 655:281–289

[22] Masrat S, Poolla R, Dipak P, Zaman MB (2021) Rapid hydrothermal synthesis of highly crystalline transition metal (Mn & Fe) doped CuSe nanostructures: applications in wastewater treatment and room temperature gas sensing. Surf Interfaces 23:100973

[23] Shitu IG, Talib ZA, Chi JLY, Kechick MMA, Baqiah H (2020) Influence of tartaric acid concentration on structural and optical properties of CuSe nanoparticles synthesized via microwave assisted method. Results Phys 17:103041

[24] Olekseyuk ID, Gulay LD, Dydchak IV, Piskach LV, Parasyuk OV, Marchuk OV (2002) Single crystal preparation and crystal structure of the Cu_2Zn/Cd, Hg/SnS_e4 compounds. J Alloy Compd 340:141–145

[25] Chen T, Zhang K, Wang H, Su W, Mehmood F, Wang T, Zhai J, Wang X, Huo T, Wang C (2020) The high thermoelectric performance of slightly Sb doped PbTe alloys. J Mater Chem C 8:1679–1685

[26] Madelung O (2004) Semiconductors: data handbook. Springer, Berlin, Heidelberg

[27] Blatt FJ (1968) Physics of electronic conduction in solids. McGraw-Hill, New York

[28] Kim H-S, Gibbs ZM, Tang Y, Wang H, Snyder GJ (2015) Characterization of Lorenz number with Seebeck coefficient measurement. APL Mater 3:041506

[29] Slack GA (1972) Thermal conductivity of II-VI compounds and phonon scattering by Fe^{2+} Impurities. Phys Rev B 6:3791–3800

[30] Chetty R, Falmbigl M, Rogl P, Heinrich P, Royanian E, Bauer E, Suwas S, Mallik RC (2013) The effect of multi-substitution on the thermoelectric properties of chalcogenide-based $Cu_{2.1}Zn_{0.9}Sn_{1-x}InxSe_4$ ($0 \leq x \leq 0.1$). Phys Status Solidi (A) 210:2471–2478